Original Article
Inner mitochondrial membrane protein MPV17 mutant mice display increased myocardial injury after ischemia/reperfusion

Ngonidzashe B Madungwe[1,2*], Yansheng Feng[1*], Abdulhafiz Imam Aliagan[1], Nathalie Tombo[1], Ferdinand Kaya[3], Jean C Bopassa[1]

[1]Department of Cellular and Integrative Physiology, School of Medicine, University of Texas Health Science Center at San Antonio, TX 78229, USA; [2]Department of Biomedical Engineering, University of Texas at San Antonio, TX 78249, USA; [3]Department of Ophthalmology, University of California Davis, CA 95616, USA. *Equal contributors.

Abstract: MPV17 is an inner mitochondrial membrane protein whose mutation results in mitochondrial DNA (mtD-NA) depletion diseases such as neurohepatopathy. MPV17 is expressed in several organs including the liver and kidneys. Here, we investigated its role and mechanism of action in cardiac ischemia/reperfusion (I/R) injury. Using isolated hearts from wild type and Mpv17 mutant (Mpv17^{mut}) mice, we found that mtDNA levels and normal cardiac function were similar between the groups. Furthermore, reactive oxygen species (ROS) generation, mitochondrial morphology, and calcium levels required to trigger mitochondrial permeability transition pore (mPTP) opening were all similar in normal/non-ischemic animals. However, following I/R, we found that mutant mice had poorer cardiac functional recovery and exhibited more mitochondrial structural damage. We also found that after I/R, Mpv17^{mut} heart mitochondria did not produce more ROS than wild type hearts but that calcium retention capacity was gravely compromised. Using immunoprecipitation and mass spectrometry, we identified ATP synthase, Cyclophilin D, MIC60 and GRP75 as proteins critical to mitochondrial cristae organization and calcium handling that interact with MPV17, and this interaction is reduced by I/R. Together our results suggest that MPV17 has a protective function in the heart and is necessary for recovery following insults to the heart.

Keywords: MPV17, mitochondrial DNA, reactive oxygen species, mPTP opening, mitochondrial calcium retention capacity, mitochondrial inner membrane proteins, ischemia/reperfusion

Introduction

In humans, the inner mitochondrial membrane (IMM) protein, referred to as MPV17, gene is located on chromosome 2p21-23, comprising eight exons encoding 176 amino acids and has been found to be expressed in the brain, kidneys, liver, spleen, and heart [1]. Almost 50 different mutations of the MPV17 gene have so far been identified in humans [2], whose phenotype manifest as liver dysfunction, neurological problems and failure to thrive in pediatric patients. The protein MPV17 is a nuclear-encoded transmembrane protein residing in the IMM, where defects in this protein have been linked with fluxes in mitochondrial reactive oxygen species (ROS) generation, ETC complex activity, mitochondrial membrane potential and pH [3, 4]. In mice, MPV17 deficiency also leads to renal disease and hearing loss,

but mice are otherwise able to survive to adulthood [1].

MPV17 was previously thought of as a peroxisomal protein [5] because of its impact on ROS production, it was later postulated to be part of a protein family that also includes peroxisomal membrane protein 2 (PXMP2), and the IMM proteins: MP-L and MPV17-Like Protein 2 (MPV17L2) [4]. In humans, mutations of the MPV17 gene have been found to cause hepatocerebral mitochondrial DNA depletion syndromes (MDS) that is an inherited disorder that can cause liver disease and neurological problems [6], which manifests as electron transport chain (ETC) dysfunction and reduced mitochondrial DNA (mtDNA) quantities. Such mutations have been observed in children of the Navajo tribe, hence it is sometimes referred to as Navajo neurohepatopathy [7]. Mutations of

murine Mpv17 result in mtDNA depletion in tissue-specific and age-dependent manners: with the kidney and brain having normal or small decreases of about 60-70% mtDNA content of the wild type, but the liver (4-5%) and muscle (20-25%) having detrimental declines [8, 9]. As a result, MPV17 has been postulated to be involved in helping maintain the mitochondrial deoxynucleoside triphosphate pool, with loss of MPV17 protein resulting in reduced dGTP and dTTP, and the eventual reduction in mtDNA in liver mitochondria [10]. Recent evidence using yeast and fibroblasts suggests that the Mpv17 gene codes for a non-selective voltage-gated channel that modulates membrane potential and is regulated by pH and redox state [4]. However, despite the phenotype of MPV17 mutation being described, particularly in the context of liver and kidney dysfunction, so far, not much is known about its mechanism of action.

Cardiac expression of MPV17 is comparable to levels observed in the kidney and liver, yet no study thus far has investigated the function of this protein in cardiac tissue. Mitochondrial ETC function and ROS generation are all essential components for normal heart function, and they are even more critical to the cardiac response to insults like ischemia/reperfusion (I/R) injury. Hence, we hypothesized that the MPV17 protein might be involved in the mitochondrial actions necessary to respond to cardiac injury.

In this study, we determined the function of the mouse Mpv17 gene in normal cardiac mitochondria and after I/R using both wild type and mutant mice. Here, we describe MPV17's role in improving cardiac functional recovery, decreasing myocardial infarct size, and maintaining mitochondrial structural integrity and function after I/R. In exploring the mechanism by which MPV17 delays opening of the mitochondrial permeability transition pore (mPTP), a key mediator of cell death after injury, we found evidence suggesting that MPV17 interacts with several critical inner mitochondrial membrane proteins. These include the mitochondrial contact site and cristae organizing system (MICOS), which regulates cristae morphology; Cyclophilin D and ETC complex V, also called ATP synthase or ATPase; as well as mitochondrial heat shock protein, glucose-regulated protein 75 (GRP75), that is necessary for endoplasmic reticulum-mitochondria Ca^{2+} transfer.

Materials and methods

Animals

All protocols followed the Guide for the Care, and Use of Laboratory Animals (US Department of Health, NIH), and received UT Health Science Center at San Antonio Institutional Animal Care and Use Committee (IACUC) institutional approval.

We used age-matched male adult wild type and full-body Mpv17 mutant mice (Mpv17[mut]) [1] (Jackson Lab, Stock No. 002208) on the CFW Swiss Webster background; between 4-6 months of age. The mutants are a transgenic strain generated by proviral insertion of a recombinant retrovirus to interfere with RNA expression of the MPV17 gene as described in [1]. Animals were genotyped using tail DNA and the following primers: Mpv17 wt/mut/f, 5'-AAC CAC TAC GGC TGG CTA GA-3', Mpv17 wt/r, 5'-GCT TCA AAG CAA ACG ACC TC-3' and Mpv17 mut/r 5'-CCT ACA GGT GGG GTC TTT CA-3'. Protocols were approved by the UT Health Science Center at San Antonio Institutional Animal Care and Use Committee and conformed to the Guide for the Care and Use of Laboratory Animals: Eighth Edition (2011) from the National Research Council.

Antibodies and reagents

All materials were purchased from Sigma-Aldrich, unless otherwise stated. Studies utilized antibodies against the following targets:

Antibody Target	Supplier	Catalog #	Concentration
MPV17	Proteintech	10310-1-AP	0.27 µg/mL
ATP synthase alpha	Invitrogen/ThermoFisher	459240	1 µg/mL
ATP synthase beta	Invitrogen/ThermoFisher	A21351	1 µg/mL
Cyclophilin D	Invitrogen/ThermoFisher	45-5900	0.5 µg/mL
MT-ATP6	Invitrogen/ThermoFisher	PA5-37129	1 µg/mL
MT-ND1	Invitrogen/ThermoFisher	PA5-75179	1 µg/mL
MT-ND2	Invitrogen/ThermoFisher	PA5-37185	1 µg/mL
GRP75	Cell Signaling Technology	3593S	1 µg/mL
GAPDH	Cell Signaling Technology	5174S	1 µg/mL
Total OXPHOS	Abcam	ab110413	6 µg/mL
Mitofilin/Mic60	Abcam	ab110329	1 µg/mL
VDAC1	EMD	MABN504	1 µg/mL
IRDye 800CW Goat anti-Rabbit	LI-COR	926-32211	0.1 µg/mL
IRDye 680RD Goat anti-Mouse	LI-COR	926-68070	0.1 µg/mL

Echocardiography

Cardiac function in normal age-matched adult mice was measured using a Vevo 1100 imaging system (Fujifilm Visualsonics) equipped with an MS-400 (18-38 MHz) linear transducer to accurately monitor the heart by measuring cardiac hemodynamic parameters and assessing heart structure [11]. Briefly, animals were intubated with oxygen supplemented with 1-2% isoflurane, and body temperature and ECG readings monitored continuously. Thoracic fur was removed using hair remover lotion and ultrasound gel applied. Recordings were taken for the following conditions: B-mode long axis, B-mode short axis, and M-mode short axis; and analysis of ejection fraction, fractional shortening, and left ventricle dimensions were conducted.

Langendorff heart perfusion

Mice hearts were prepared and perfused as previously described in [12]. Briefly, mice were anesthetized using ketamine (80 mg/kg i.p.) and xylazine (8 mg/kg i.p.) before hearts were carefully removed and arrested in cold (4°C) Krebs Henseleit bicarbonate buffer (KH) solution with the following composition (in mM): glucose 11, NaCl 118, KCl 4.7, $MgSO_4$ 1.2, KH_2PO_4 1.2, $NaHCO_3$ 25 and $CaCl_2$ 3, pH 7.4. The hearts were retrograde-perfused with KH buffer bubbled with 95% O_2/5% CO_2 at 37°C using the Langendorff apparatus at a constant rate (3 ml/min). Equilibration lasted 30 minutes before global ischemia was induced for 30 minutes by stopping buffer flow and then followed by reperfusion for 20 minutes (mitochondrial isolation) or 120 minutes (cardiac function and infarct size measurement). Mitochondrial function tests and Western blot were conducted on mitochondria after 20 min reperfusion, but as we did not observe any protein level differences at this time point, the co-immunoprecipitation experiments used mitochondria at 120 min reperfusion that is sufficient for protein changes to become observable. Acceptable hearts were ones that reached a minimum left ventricular developed pressure (LVDP) of 80 mmHg at the end of the basal perfusion (pre-ischemia). Sham hearts were not subjected to I/R.

Isolated heart functional measurements

Cardiac function was recorded as previously described in our articles [13, 14] using a 1.4F SPR-671 pressure sensitive catheter (Millar, Inc.) that was inserted into the left ventricle (LV) via a left atrial incision. Recordings for LV end-systolic pressure (LVSP), LV end-diastolic pressure (LVEDP), and heart rate (HR) were taken using Powerlab software (ADInstruments) as described in [15]. Readings for LV developed pressure (LVDP = LVSP - LVEDP) and the Rate-Pressure Product (RPP = LVDP × HR) were directly calculated from the recordings at the end of reperfusion by a blinded investigator.

Myocardial infarct size measurements

At the end of reperfusion, hearts were cut into five transverse slices parallel to the atrio-ventricular groove as previously described [13], followed by incubation for 10 minutes in 2% triphenyltetrazolium chloride at 37°C to differentiate viable (red) from infarcted (white) heart tissue. Sections were then fixed with 4% paraformaldehyde before being imaged. Planimetry using Adobe Photoshop CS6 was used to quantify the necrotic area by a blinded investigator.

LDH release assay

Release of lactate dehydrogenase (LDH) in the coronary effluent, a marker for cardiac injury, was measured using an LDH Assay Kit (Abcam, catalog no: ab197000) and according to the supplier's instructions. Briefly, effluent from ischemic hearts was collected over 30 min reperfusion, and assayed for LDH activity using the assay buffer, PicoProbe and substrate mix. Fluorescence was measured at Ex/Em = 535/587 nm.

Mitochondrial isolation

Mitochondria were isolated from mice hearts at 4°C as described previously in [15]. Sections were placed in isolation buffer A (in mM): sucrose 70, mannitol 210, EDTA 1 and Tris-HCl 50, pH 7.4, followed by mincing and homogenization in the same Buffer A (0.1 g of tissue/ml of buffer). The resulting homogenate was centrifuged at 1300 × g for 3 minutes in a Galaxy 20R centrifuge (VWR) and the supernatant was centrifuged again at 10,000 × g for 10 minutes. The mitochondrial pellet obtained was then resuspended in isolation Buffer B (in mM): sucrose 150, KCl 50, KH_2PO_4 2, succinic acid 5, and Tris/HCl 20, pH 7.4. Total protein concentration was calculated using the BCA assay kit (ThermoFisher).

DNA extraction and quantification

Total DNA was isolated from whole mice hearts using the DNeasy Blood and Tissue kit (Qiagen), and concentration determined using spectrophotometry (Biodrop). To quantify mtDNA in relation to nuclear DNA, we amplified regions of the mitochondrial gene CoxII and the nuclear gene App1 as described in [10] using real time quantitative PCR and the following primers: mCoxII-f, 5'-GAG CAG TCC CCT CCC TAG GA-3', mCoxII-r, 5'-GGT TTG ATG TTA CTG TTG CTT GAT TT-3', nApp1-f, 5'-CGG AAA CGA CGC TCT CAT G-3', and nApp1-r, 5'-CCA GGC TGA ATT CCC CAT-3'. PCR samples along with PowerUp SYBR Green Master Mix (ThermoFisher) were run on a 7500 Fast Real-Time PCR system (Applied Biosystems) to obtain ΔCT (cycling threshold values).

Mitochondrial H_2O_2 measurement

Mitochondrial ROS production was measured spectrofluorometrically using its analog H_2O_2 in 100 µg mitochondrial extract at 560 nm excitation and 590 nm emission. Samples were incubated with the H_2O_2-sensitive dye Amplex red reagent (1 µM) (ThermoFisher) and horseradish peroxidase (0.345 U/mL) in a buffer solution containing (in mM): 20 Tris, 250 sucrose, 1 EGTA, 1 EDTA, and 0.15% bovine serum albumin adjusted to pH 7.4 at 30°C with continuous stirring. H_2O_2 production was calculated using a standard curve of H_2O_2 concentration and fluorescence intensity. To activate the ETC complexes I and II, sodium salts of glutamate/malate (3 mM) and succinate (3 mM) were used, respectively, as previously described [13].

Ca^{2+}-induced mitochondrial permeability transition pore (mPTP) opening

Resistance to calcium-induced mitochondrial permeability transition pore (mPTP) formation was assessed using *in vitro* Ca^{2+} overload in isolated mitochondria as previously described [16, 17]. Using 0.1 µM of the Ca^{2+} sensitive dye, calcium green-5N (ThermoFisher), we recorded free Ca^{2+} concentration using excitation and emission wavelengths set at 500 and 530 nm, respectively. Samples of 500 µg of isolated mitochondrial protein, in 2 mL of Buffer B were incubated for 90 seconds in a fluorescence spectrophotometer (Hitachi) set at 30°C with constant stirring. For experiments with cyclosporin A, (CsA), mitochondria were incubated in 2 mL of Buffer B supplemented with 10 µM CsA. We applied pulses of $CaCl_2$ (10 µmoles) every 60 seconds to the cuvette which induce a fluorescence peak when bound reversibly to calcium green-5N dye, followed by a decrease as mitochondria take up the Ca^{2+}. As calcium load increases, the extra-mitochondrial Ca^{2+} concentration starts to accumulate, a signal of lower capacity for mitochondrial Ca^{2+} uptake, eventually leading to mPTP opening and the massive release of mitochondrial Ca^{2+}. The amount of Ca^{2+} required to trigger this massive Ca^{2+} release was recorded as the Ca^{2+} retention capacity (CRC) of the sample, a potent indicator of mPTP sensitivity to Ca^{2+}. CRC was expressed as nmol of $CaCl_2$ per mg of mitochondrial protein.

Western blot analysis

Equal concentrations of lysed tissue and isolated mitochondria were loaded into 4-20% Tris-glycine gels (Bio-Rad) as recently described in [18]. Electrophoresis was carried out for 90 min at 100 V of constant voltage, followed by blotting onto nitrocellulose membranes at constant 90 V for 80 min. Membranes were blocked with 5% blotting-grade blocker solution (BioRad), probed overnight with various primary antibodies at 4°C and visualized using IRDye secondary antibodies and an Odyssey CLx digital imaging system (LI-COR Biotechnology).

Immunoprecipitation

Isolated mitochondria was pelleted and resuspended in lysing buffer made up of: 50 mM Tris-HCl, 150 mM NaCl, 1 mM Na_3VO_4, 0.5 mM NaF, 0.1% NP-40, 0.25% Na-deoxycholate, at pH 7.4 and supplemented with a Protease Inhibitor Cocktail tablet (Roche, 1 tablet/50 ml). Samples were rotated at 4°C for 3 h before being pelleted and the supernatant sonicated and quantified using the BCA assay (ThermoFisher). Equal quantities of each sample (1 mg) were pre-cleared with protein A/G agarose resin (ThermoFisher) before being added to fresh resin with specific antibodies (MPV17, CypD, ATPase α, ATPase β, GRP75; supplier numbers listed in the table above). After overnight spinning at 4°C, samples were washed 8 × with lysis buffer before 1 × Laemmli buffer with β-mercaptoethanol was added. Samples

were heated in boiling water before being run on a 4-20% Tris-glycine gel and probed by Western blot analysis.

Transmission electron microscopy

To analyze mitochondrial morphology in normal and I/R mice hearts, samples were fixed in a phosphate buffered solution of 4% formaldehyde with 1% glutaraldehyde, and stored at 4°C overnight as described in [19]. Tissue sections were washed with PBS, post-fixed in 2% (wt/vol) osmium tetroxide for 2 h at room temperature, and dehydrated in a graded alcohol series before being embedded in Eponate 12 medium. The blocks were cured at 60°C for 48 h, and 70 nm sections were cut using an ultramicrotome, mounted on Formvar-coated grids and double-stained with uranyl acetate and lead citrate. The resulting samples were analyzed and imaged using a JEOL 1230 transmission electron microscope. Mitochondria were classified as 'damaged' if they had more than 50% disorganized/destroyed cristae structure. Mitochondrial area was calculated using ImageJ software.

Protein identification/relative quantification by mass spectrometry

We immunoprecipitated MPV17 protein from non-ischemic wild type isolated mitochondria samples. Proteins eluted from the MPV17 pull-down were separated by SDS-PAGE prior to mass spectrometry analysis. Gels were run ~ 2 cm and then regions of interest in each lane were subdivided into slices that were individually reduced/alkylated and digested with trypsin. The digests were analyzed by HPLC-electrospray ionization-tandem mass spectrometry on an Orbitrap Velos Pro (Thermo Scientific). Mascot (Matrix Science) was used to search the UniProt_mouse database and a database of common contaminants. The Mascot results files for the gel slices in each lane were combined for subset searching of the identified proteins by X Tandem, cross-correlation with the Mascot results, and determination of protein and peptide identity probabilities by Scaffold (Proteome Software). Relative quantities were determined by spectral counting.

Statistical analysis

Data is presented in bar graphs expressed as means, and error bars are the standard errors of the mean (± SEM). Comparisons were conducted using the Student's t-test and two-way ANOVA with post-hoc Dunnett's, Tukey's, and Sidak's corrections for multiple comparisons, where appropriate, using Prism 6 (Graphpad Software). A difference of P < 0.05 was considered to be statistically significant.

Results

Absence of functional MPV17 does not significantly affect mtDNA quantity in the heart and overall heart function in normal adult mice

Mpv17^{mut} mice were genotyped and checked using Western blot for functional MPV17 protein (**Figure 1A**, **1B**). As Mpv17 mutation results in the phenotype of mtDNA depletion syndromes particularly in the liver, we confirmed this by checking the mtDNA levels in the liver, heart and kidneys (**Figure 1C-E**). As expected, Mpv17^{mut} liver had significantly less mtDNA at 7% of the wild type (WT), while the kidneys had slightly less mtDNA than the WT (89% of the WT), all in line with the tissue-specific mtDNA differences observed by other investigators [9, 10]. For the heart, we found that cardiac mtDNA levels were not significantly different between WT and Mpv17^{mut}, with the Mpv17^{mut} hearts appearing to have slightly more mtDNA than the WT (1174 AU for WT versus 1447 AU for Mpv17^{mut}). We then examined whether Mpv17 mutation affects the overall heart weight (HW) as a function of the body weight (BW) in adult mice and here we also found that the ratio HW/BW was not different in Mpv17^{mut} animals as compared to WT (**Table 1**). Echocardiography to assess normal heart function between age-matched WT and Mpv17^{mut} animals also showed that both groups exhibit similar hemodynamic function (**Table 1**). In fact, despite small differences in left ventricle (LV) dimensions and slightly lower heart rates in Mpv17^{mut} animals, the ejection fraction and fractional shortening were not significantly different between the WT and Mpv17^{mut} groups.

Mpv17 mutation decreases cardiac functional recovery and increases myocardial infarct size after I/R

In order to determine the functional significance of MPV17 in mice hearts in stress conditions, we perfused isolated hearts from WT and Mpv17^{mut} animals using a Langendorff retrograde perfusion system and recorded cardiac
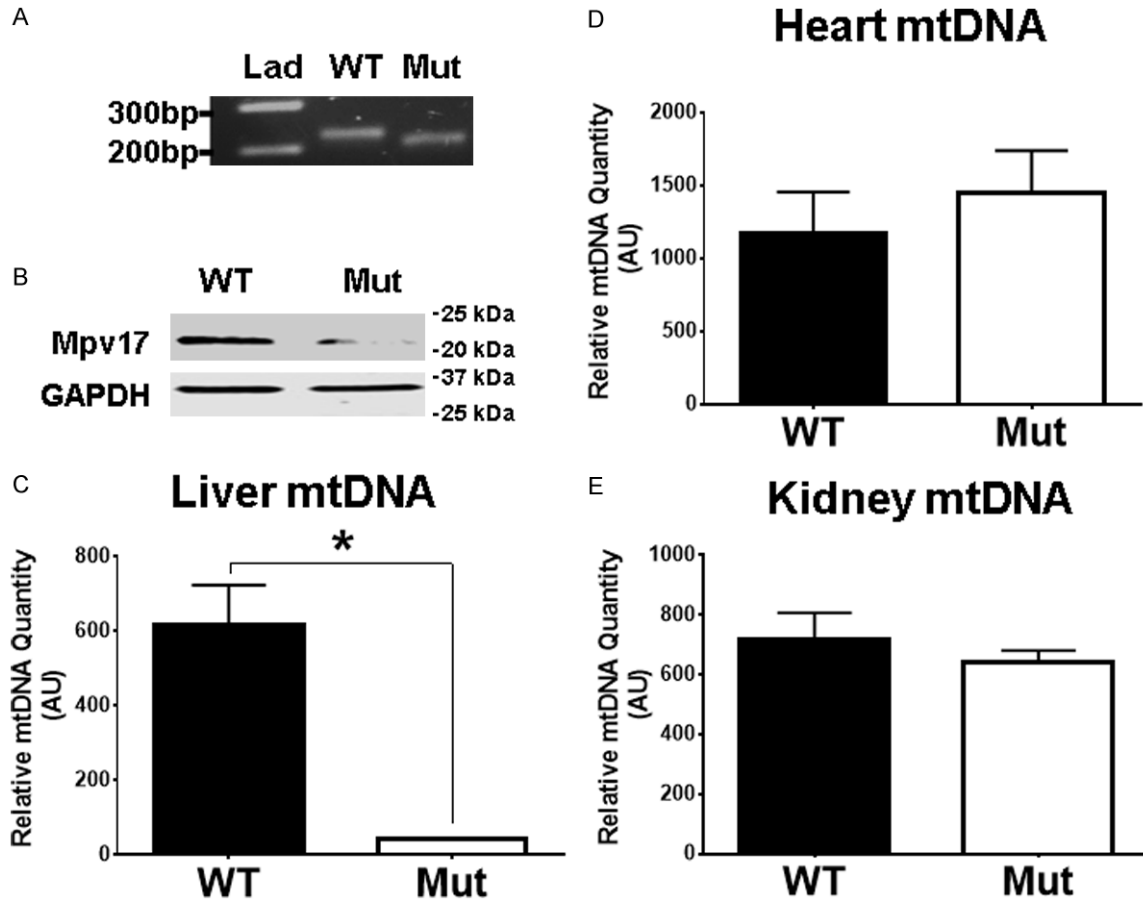
Figure 1. Characterization of MPV17 in normal WT and *Mpv17^mut* mice. A. Standard PCR results from mice-tail genotyping in WT and *Mpv17^mut*. The wild type band is at 232 bp and *Mpv17^mut* band is at 200 bp. B. Immunoblot showing lack of functional MPV17 protein in mutant mice heart mitochondria as compared to WT mitochondria. C. Bar graph showing mtDNA levels in WT and *Mpv17^mut* mice livers. *Mpv17^mut* had significantly decreased mtDNA, which is the hallmark phenotype of mtDNA disease in mutant mice. D. Bar graph showing no significant changes in mtDNA levels in mice hearts between WT and *Mpv17^mut*. E. Bar graph showing that mtDNA levels in mice kidneys are not greatly affected between WT and *Mpv17^mut*. Values are mean ± SEM; *$P < 0.05$ WT *versus Mpv17^mut*, n = 5/group.

Table 1. Data obtained from echocardiography on intact adult age-matched mice (in vivo)

Parameter	WT	MPV17^mut
HW/BW	0.00405 ± 0.000138	0.00399 ± 0.0000912
Ejection Fraction (%)	68.4 ± 6.06	77.5 ± 3.44
Fractional Shortening (%)	38.9 ± 5.38	45.6 ± 3.39
Heart Rate (bpm)	482 ± 36.2	416 ± 15.5
LVID; d (mm)	3.83 ± 0.103	3.06 ± 0.106*
LVID; s (mm)	2.35 ± 0.245	1.68 ± 0.158*

We observed slight differences in internal dimensions but no major functional differences. LVID; d/s, left ventricle internal diameter; diastole or systole; HW: heart weight; BW: body weight. Values are mean ± SEM; *$P < 0.05$ WT versus MPV17^mut, n = 5-6/group.

function pre- and post-ischemia (**Figure 2A**). While recordings were similar in both groups before the initiation of global normothermic ischemia, the Mpv17^mut hearts demonstrated significantly reduced ability to recover from the insult (**Figure 2A**, **2B**). As shown in **Figure 2C**, Mpv17^mut mice hearts had reduced cardiac functional recovery as measured using the rate-pressure product (RPP) recovery at the end of 120 min reperfusion relative to pre-ischemia. In fact, while the RPP at the end of reperfusion in WT averaged 16,773 mmHg/min, it was reduced to 10,427 mmHg/min in Mpv17^mut hearts (**Figure 2B**). Further, we deter-
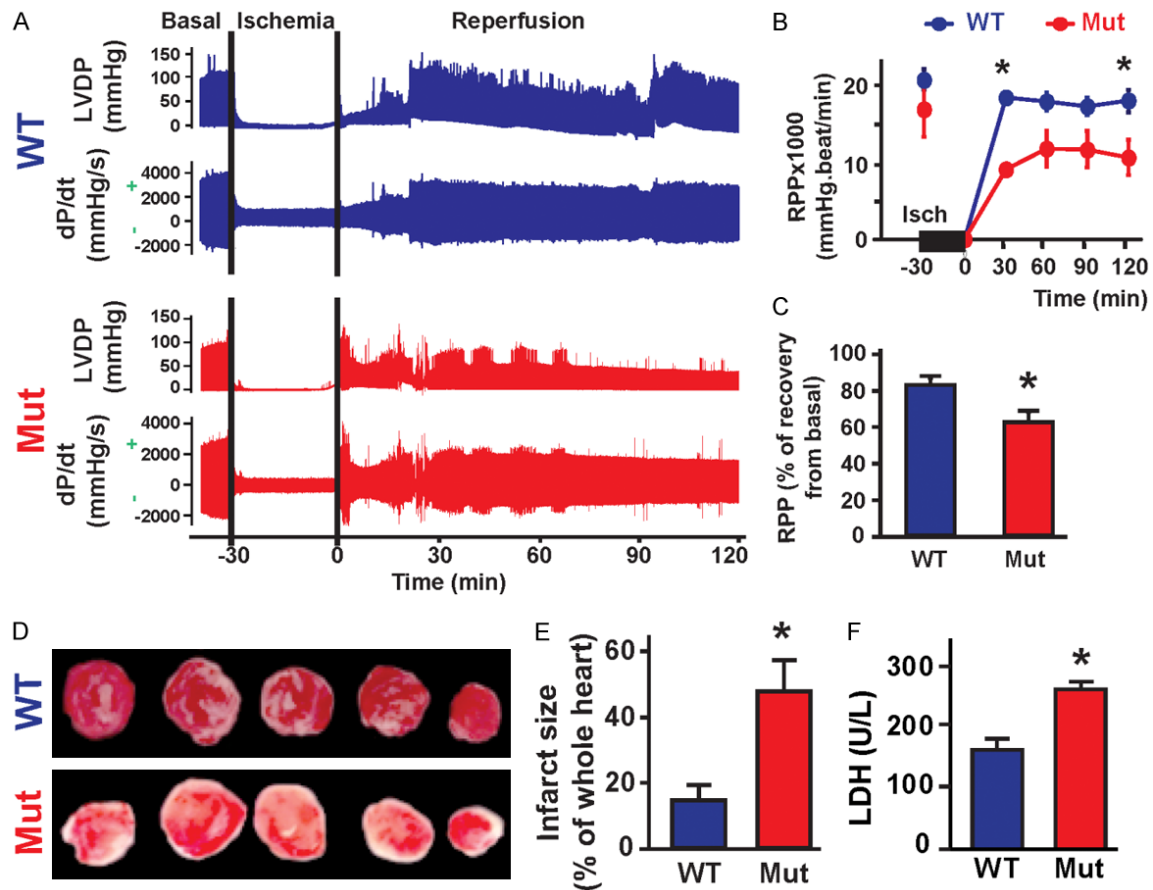
Figure 2. *Mpv17^mut* mice exhibit reduced cardiac function recovery and increased myocardial infarct size after I/R. A. Typical recording of isolated perfused heart function from WT and *Mpv17^mut* mice. Traces show the cardiac function from pre-ischemia to the end of 120 min reperfusion showing *Mpv17^mut* hearts recover less during reperfusion as compared to WT. Blue graphs show left ventricle developed pressure (LVDP) and change in pressure (dP/dt) for WT, while those for *Mpv17^mut* are in red. B. Time course of changes in rate-pressure product (RPP) showing a better improvement of WT hearts function recovery during reperfusion compared to *Mpv17^mut* hearts. C. Graph quantifying the decrease in cardiac functional % Recovery of *Mpv17^mut* compared to WT, as measured by the RPP pre-ischemia versus at 120 min reperfusion. D. Representative images from 5 slices of the same heart showing increased myocardial infarct size in *Mpv17^mut* compared to WT mice, measured at the end of 120 min reperfusion in isolated infarcted zone and red areas indicate viable cells. E. Bar graph showing an increase of myocardial infarct size in the Mpv17^mut group compared to the WT group. F. Bar graph showing increased lactate dehydrogenase (LDH) release in Mpv17^mut hearts compared to WT. Values are mean ± SEM; *P < 0.05 WT versus Mpv17^mut; n = 5/group.

mined the myocardial infarct sizes obtained from hearts subjected to I/R injury at the end of 2 h reperfusion. **Figure 2D** represents an example of five slices of the same heart for WT and Mpv17^mut animals. We found that Mpv17^mut mice hearts had significantly larger infarcted regions, as shown by the increased white area, compared to WT hearts (48% in Mpv17^mut versus 14% in WT) (**Figure 2E**), suggesting an important role for MPV17 in the cardiac response to I/R injury. In line with these results, we found that the release of lactate dehydrogenase (LDH) enzyme in the coronary effluent

was increased in the Mpv17^mut compared to the WT hearts (**Figure 2F**).

Cardiac mitochondria from Mpv17^mut mice have more damaged cristae after I/R

MPV17 protein resides in the inner mitochondrial membrane (IMM), which creates the folded cristae that are unique to mitochondria. We, therefore, analyzed cristae morphology using electron microscopy images of fixed heart tissue sections (**Figure 3A**) and isolated mitochondria (**Figure 3D**) for WT and Mpv17^mut, both in normal and post-ischemic conditions. In line
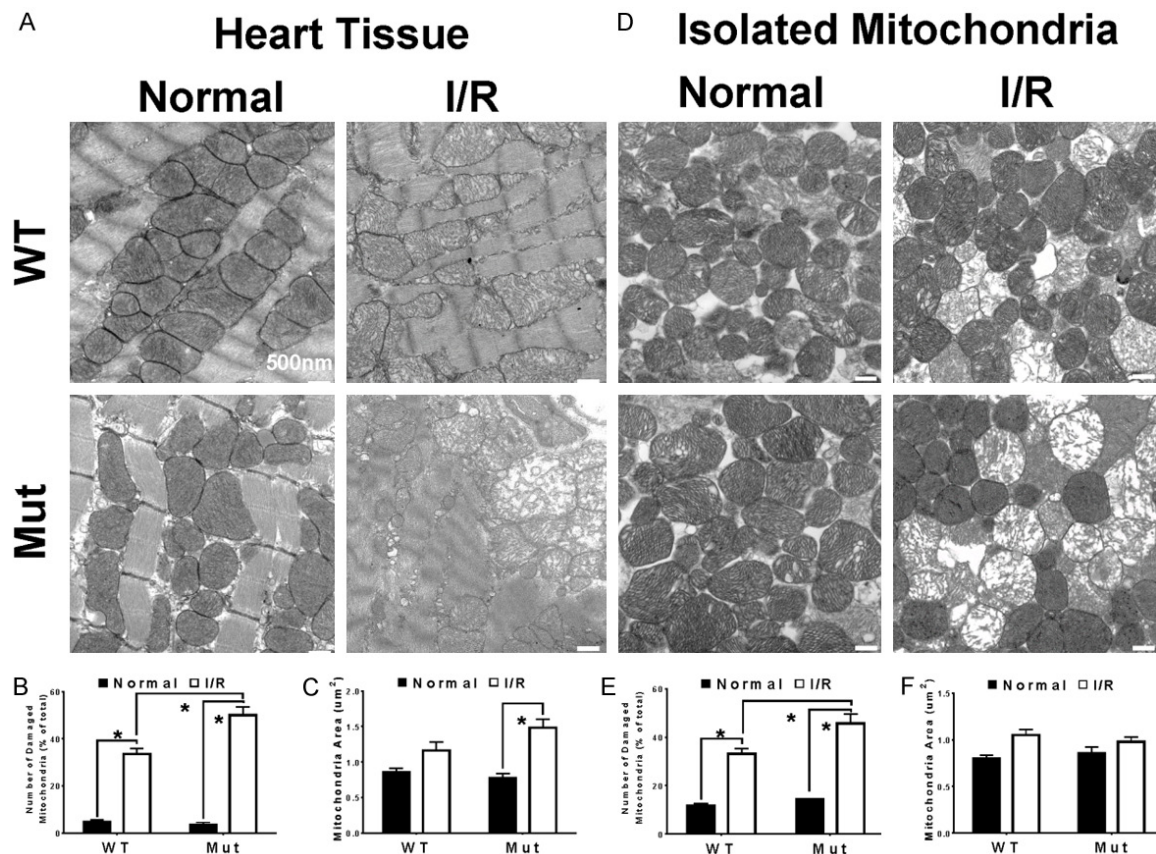
Figure 3. *Mpv17^mut* hearts mitochondria preserve a better ultrastructure compared to WT after I/R. (A) Electron microscopy images showing that in normal/non-ischemic condition, WT and *Mpv17^mut* heart tissues and isolated mitochondria (D) have similar ultrastructure and normal cristae organization. However, following I/R, *Mpv17^mut* mitochondria in both heart tissue (A) and isolated mitochondria (D) display greater damage to cristae morphology as well as increased swelling. (B-F) Bar graphs quantifying the number of damaged mitochondria and average mitochondrial area in tissue and isolated mitochondria images. Values are mean ± SEM; *P < 0.05; n = 6-10 images each heart.

with the observations of near-normal cardiac function before ischemia, we found that cristae morphology in Mpv17^mut and WT samples was similar and organized in normal heart tissue and in isolated mitochondrial fractions (**Figure 3A**, **3D**). However, following ischemic injury, whole heart sections from Mpv17^mut mice hearts had more enlarged mitochondria with damaged cristae morphology versus WT (33% damaged mitochondria in WT versus 50% damaged in Mpv17^mut; **Figure 3B**). Accordingly, when focusing on isolated mitochondria from the Mpv17^mut mice after I/R, the cristae clearly exhibited greater disruption and disorganization compared to their WT counterparts (33% damaged mitochondria in WT versus 46% damaged in Mpv17^mut; **Figure 3E**) suggesting that MPV17 may help to stabilize cristae structure. In heart sections, MPV17^mut had more swollen mito-

chondria than WT (**Figure 3C**). However, this was not observed in isolated mitochondria (**Figure 3F**) possibly due to the differential centrifugation used to isolate mitochondria, as the protocol would have resulted in similar-sized mitochondria grouping together.

Mitochondria from Mpv17^mut mice produce ROS at levels similar to wild type but are less resistant to calcium-induced mPTP opening following I/R

Opening of the mPTP is a key event leading to apoptosis and necrosis that can be triggered by either increased ROS production or calcium overload [20]. To assess the role of ROS in the observed cell death, we next measured ROS production from WT and Mpv17^mut heart mitochondria and surprisingly found that they pro-
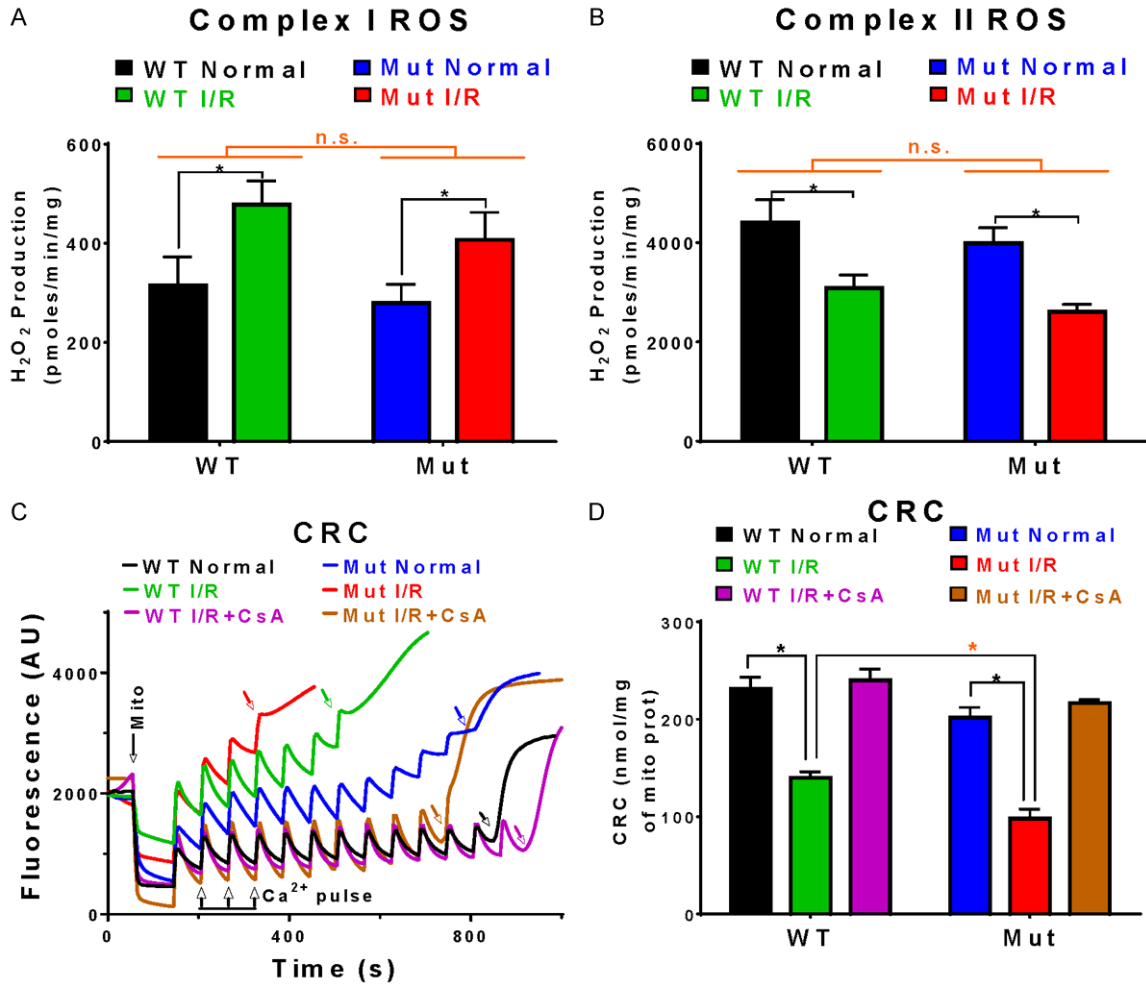
Figure 4. *Mpv17^mut* heart mitochondria display reduced ROS production and delay of the mPTP opening after I/R. A. Bar graph showing changes in H_2O_2 release from complex I stimulation between normal and I/R mitochondria. Note that no significant changes were observed between WT and *Mpv17^mut*. B. Bar graph showing no significant changes in H_2O_2 release from complex II stimulation between normal and I/R mitochondria in WT and *Mpv17^mut*. C. Typical readings for the calcium overload required to induce the mPTP opening (colored arrows) of isolated mitochondria from WT normal (black trace), WT I/R (green trace), *Mpv17^mut* normal (blue trace), *Mpv17^mut* I/R (red trace) WT I/R + CsA (purple trace) and Mpv17^mut I/R + CsA (brown trace). D. Bar graphs showing mitochondrial calcium retention capacity (CRC) measured from isolated mitochondria and how *Mpv17^mut* have significantly decreased CRC compared to WT after I/R. Values are mean ± SEM; *P < 0.05; n = 6/group.

duced ROS at similar levels both before and after ischemic insult (**Figure 4A**, **4B**). Although ROS are generally considered damaging to the cell, they are also known to function as essential signaling molecules that can upregulate cardiac protection [21]. From our previous studies [12], we have shown that after cardiac I/R insult, ROS from complex I increases, causing damage; but that oppositely, ROS from complex II which we found to be cardioprotective, was decreasing. In this study, we also observed an increase in Complex I ROS and a decrease in complex II ROS after I/R. However, these chang-

es did not result in significant differences between Mpv17^mut and WT cardiac mitochondria (46-52% increase in complex I ROS generation in both groups and 30-34% decrease in complex II ROS in both groups) (**Figure 4A**, **4B**).

To assess the ability of mitochondria from WT and Mpv17^mut hearts to resist mPTP opening due to calcium overload, we assessed calcium retention capacity (CRC) of isolated mitochondria both before and after ischemia. As shown in **Figure 4C**, **4D**, normal/non-ischemic Mpv-17^mut mitochondria respond similarly to WT

mitochondria in their ability to absorb Ca^{2+} (WT-normal 231 nmol/mg of mito protein versus Mpv17^{mut} normal 202 nmol/mg of mito protein), with a higher calcium retention capacity reflecting greater resistance to mPTP opening. Post-ischemia, CRC is expected to decrease as mitochondria will be suffering due to I/R stress and Ca^{2+} influx [19], consistently, we observed that Mpv17^{mut} mitochondrial CRC declined significantly more than WT CRC (**Figure 4D**). The post-ischemic CRC values for Mpv17^{mut} averaged 98 nmol/mg of mito protein while those for WT were 140 nmol/mg of mito protein, hence a 39% decrease in WT but a 51% decrease in Mpv17^{mut} CRC. To further confirm the involvement of mPTP opening in the mechanism leading to increased myocardial infarct size after I/R in Mpv17^{mut}, we treated WT and Mpv17^{mut} hearts with Cyclosporin A [22], well known to delay the opening of mPTP via its binding to Cyclophilin D, a regulator of mPTP opening [23]. We found that Cyclosporin A treatment brings back mitochondrial CRC to respective sham levels suggesting that Mpv17 mutant mitochondria display a higher sensitivity calcium overload required to induce mPTP opening compared WT mitochondria (**Figure 4C**, **4D**). Together, these results suggested an important role for MPV17 in how mice heart mitochondria respond to calcium overload after ischemic insult. Additionally, Western blot analysis confirmed that our I/R model causes cell death by the increasing the release of cytochrome C and apoptosis-inducing factor (AIF) into the cytosol (**Figure 6G**) probably as a consequence of mPTP opening. However, we did observe that while release of cytochrome C in Mpv17^{mut} was comparable to the WT after I/R, the Mpv17^{mut} released more AIF into the cytosol suggesting an AIF-dependent mechanism being dominant in the Mpv17^{mut} group (**Figure 6G**). Taken together, these findings suggest that mitochondria are more sensitive to Ca^{2+} challenge when MPV17 is mutated and there are no significant differences in cardiac ROS production between WT and Mpv17^{mut} groups.

MPV17 mutation does not significantly affect quantity of nuclear and mitochondrial-encoded ETC subunits in the heart

As mtDNA codes for some ETC subunit proteins in mitochondria, MPV17 mutation in hepatopathic diseases has been reported to be char-

acterized by defects in the ETC 4. However, we found that MPV17 mutation did not significantly affect cardiac mtDNA levels (**Figure 1D**) or ROS production (**Figure 4A**, **4B**). To further confirm this lack of impact on the cardiac ETC in mice, we evaluated the impact of MPV17 mutation on ETC subunit protein levels in mitochondria both before and after I/R. We examined the relative quantities of ETC subunits in Mpv17^{mut} versus WT mitochondria. From results shown in **Figure 5A**, **5B**, we did not observe any significant differences to the nuclear-encoded ETC subunits: NDUFB8 (complex I), SDHB (complex II), UQCRC2 (complex III) and ATP5A (complex V/ATPase). We also did not observe any significant differences in the mtDNA-encoded subunits: MT-ND1 and MT-ND2 (complex I) (**Figure 5B**, **5C**), MT-CO1 (complex IV) (**Figure 5A**) and MT-ATP6 (complex V) (**Figure 5C**). Taken together, MPV17 mutation does not modify cardiac mtDNA levels, ETC subunit expression, and ETC production of ROS.

MPV17 protein interacts with ATP synthase, MICOS, Cyclophilin D, and Grp75

From studies in yeast, it has been suggested that MPV17 is part of a large multimeric protein complex (>600 kDa), but the exact identity of this complex has yet to be revealed [24]. Thus, using mass spectrometry on immunoprecipitated pulldowns of MPV17 from WT cardiac mitochondria samples, we sought to determine what proteins interact with MPV17. Interestingly, we found that MPV17 interacts with a large number of proteins in mitochondria and the IMM (listed in **Table 2**) that include ATP synthase subunits α and β, the mitochondrial contact site and cristae organizing system (MICOS) subunits, the mPTP regulator, Cyclophilin D, and the Hsp70 family member, glucose-regulated protein 75 (GRP75). Here, we noted that fragment hits for the F1 unit of ATP synthase (complex V) were most abundant. Proteins selected for further study included the F1FO-ATP synthase, which had the most hits, as well as Ca^{2+}-related proteins as we had observed a Ca^{2+}-dependent impact on mPTP opening (**Figure 4**).

To ascertain the interactions with these key mitochondrial proteins, we used co-immunoprecipitation followed by Western blot analysis, which confirmed the interaction between
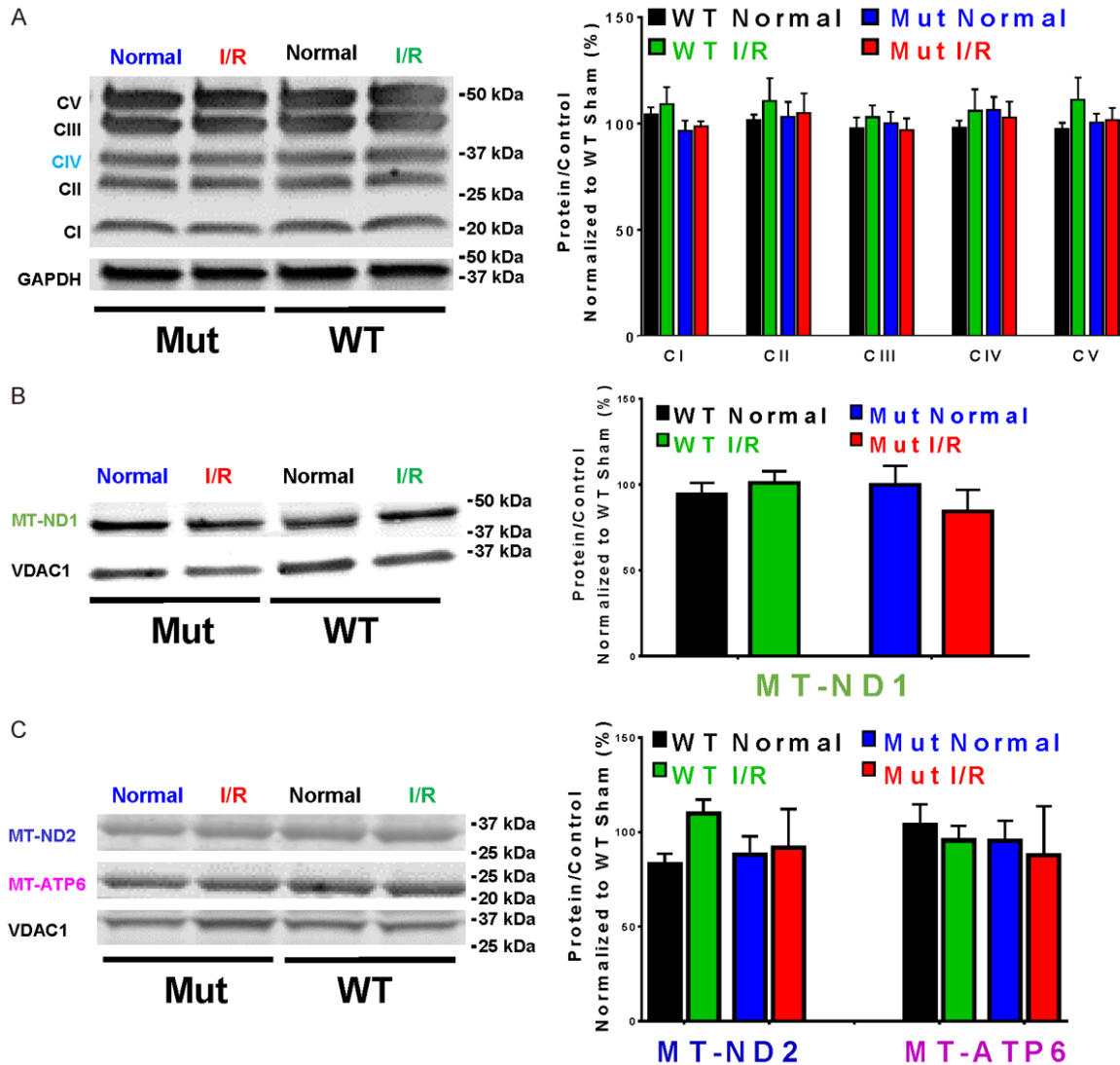
Figure 5. Protein expression analysis of ETC subunits encoded by nuclear and mitochondrial DNA. A. Western blot analysis showing no changes in expression behavior of ETC subunits encoded by nuclear DNA. Complex I (CI, NDUFB8), complex II (CII, SDHB), complex III (CIII, UQCRC2), complex IV (CIV, MTCO1), complex V (CV, ATP5A) and GAPDH. Note, the CIV subunit shown is encoded by mtDNA. B. Bar graph quantifying the lack of difference in expression between nuclear-encoded ETC subunits. C. (Left) Western blot analysis showing no changes in mtDNA-encoded ETC subunits MT-ND1, MT-ND2 and MT-ATP6; (Right) Bar graphs showing quantification of Western blot results. Values are mean ± SEM; n = 5/group.

ATPase subunits (α, β), Cyclophilin D (Ppif), and GRP75 (Hspa9/mortalin) proteins with MPV17 (**Figure 6A**). And to further establish these protein connections, we performed reverse co-immunoprecipitation by pulling down the ATPase subunits, Cyclophilin D, and GRP75, and then probing for MPV17 (**Figure 6B-F**).

Discussion

In this paper, we report that mice with mutation in their inner mitochondrial membrane protein MPV17 (MPV17[mut]) exhibit larger myocardial infarct size and impaired cardiac functional recovery after I/R as compared to WT. The mechanism of this cardiac dysfunction is associated with increased mitochondrial sensitivity to calcium required to trigger mPTP opening that could result from the decrease of the interactions between MPV17 with several inner mitochondrial membrane proteins. We also report that the cardio-deleterious effects of MPV17 mutation are not associated with any changes
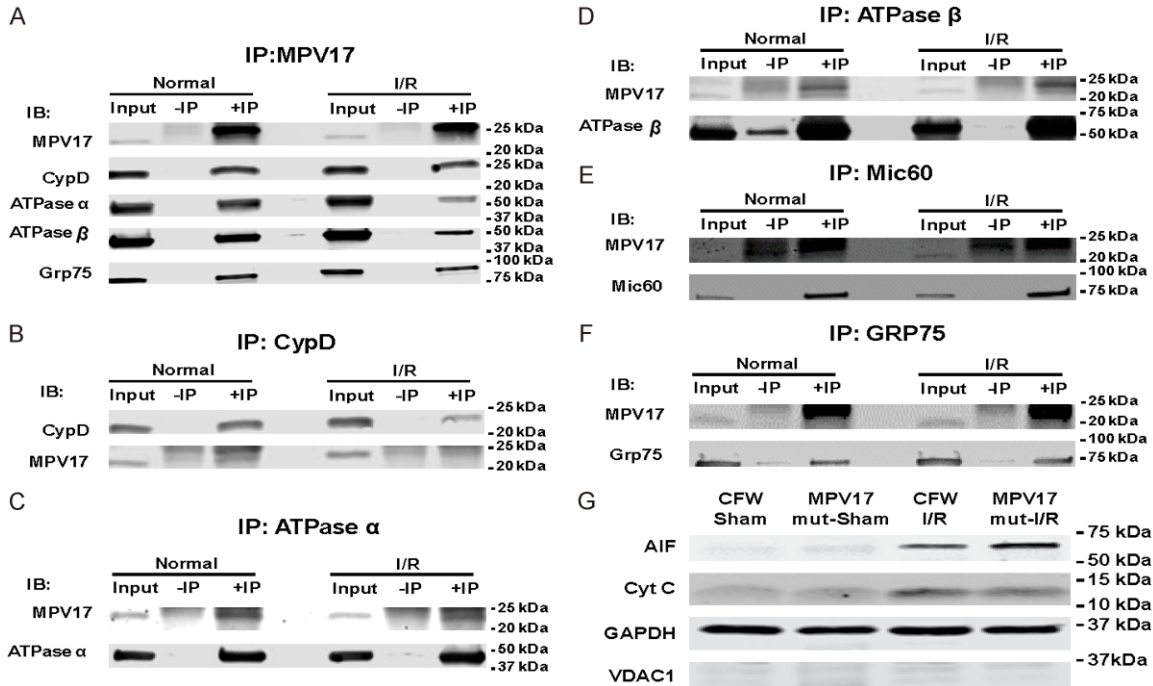
Figure 6. Interacting partners of MPV17 levels are reduced in *Mpv17^mut^* after I/R compared to WT. A. Immunoblots of proteins pulled down from normal WT mice heart mitochondria using anti-MPV17 antibody. B-F. Reverse co-immuno-precipitation of the candidate proteins confirming their interaction with MPV17. G. Immunoblot showing an increase in the release of cytochrome C (Cyt C) and apoptosis inducing factor (AIF) into the cytosol after I/R compared to sham (normal). Note that the *Mpv17^mut^* released more AIF than WT after I/R. VDAC1 expression was used to confirm the purity of the cytosol due to the absence of mitochondrial protein, n = 3/group.

in cardiac mtDNA levels, ETC protein expression and mitochondrial reactive oxygen species (ROS) production.

Mitochondria are involved in a wide range of cellular activities, including energy production, calcium homeostasis, chemical signaling, and regulation of cell death [25-27]. There is growing recognition of the importance of mitochondrial proteins, especially in the IMM, and the roles they play in health and pathophysiology [28]. One of these key proteins, MPV17, has been abundantly studied in humans (in the kidney, brain, and liver), as well as in mice, zebrafish, and yeast [2, 29]. Despite all this, the exact function and mechanism of action of mammalian MPV17 is still unclear, particularly in the heart where organized cristae structure and ETC reliability are essential for heart function [19, 30]. Here, we found that mice hearts with mutated MPV17 contain comparable mtDNA levels to those found in WT hearts (**Figure 1D**). This was not surprising given the lack of cardiac functional differences between normal adult

Mpv17^mut^ and WT mice (**Table 1**) in basal conditions. This also was in line with the absence of a negative cardiac phenotype observed by other investigators, besides an age-related increase in hypertension and tachycardia [31]. It has also been reported that mtDNA levels in Mpv17^mut^ mice exhibit tissue-specific [4] and age-related variability [9], which we also observed in the liver and kidneys (**Figure 1C**, **1E**). Here, we report that adult Mpv17^mut^ mice exhibit normal cardiac function with normal mitochondrial morphology, comparable to WT (**Figures 1**, **3**; **Table 1**). However, following I/R insult, these hearts are less able to recover function (**Figure 2A-C**), display significant increases in myocardial infarct size (**Figure 2D**, **2E**), release more LDH (**Figure 2F**) and have more damaged mitochondria (**Figure 3**). These findings suggest that MPV17's impact is not prominent in the normal heart but after I/R, MPV17 mutation results in cardio-deleterious effects.

I/R injury is strongly associated with mitochondrial dysfunction via the dysregulation of the

Table 2. Summary of proteins identified by unique peptide matches using mass spectrometry

Protein	Gene	MW (kDa)	Total Spectra from Input	Total Spectra from anti-MPV17 Pulldown
ATP synthase subunits				
ATP synthase subunit alpha	Atp5a	60	1429	195
ATP synthase subunit beta	Atp5b	56	1737	105
ATP synthase subunit gamma	Atp5c1	33	189	14
ATP synthase subunit O	Atp5o	23	269	12
ATP synthase F (0) complex subunit B1	Atp5f1	29	240	12
ATP synthase subunit d	Atp5h	19	163	7
ATP synthase subunit e	Atp5i	8	136	4
ATP synthase subunit delta	Atp5d	18	78	2
ER-Mitochondrial connection/Ca^{2+} handling/stress proteins				
Grp75/Stress-70 protein, mitochondrial	Hspa9	73	347	128
78 kDa Glucose-regulated Protein	Hspa5	72	88	28
Heat shock cognate 71 kDa protein	Hspa8	71	109	17
Hsp60/60 kDa Heat Shock Protein, mitochondrial	Hspd1	61	436	16
Sarcoplasmic/endoplasmic reticulum calcium ATPase 2	Atp2a2	115	250	55
Voltage-dependent anion channel protein 1	Vdac1	31	481	5
Voltage-dependent anion channel protein 2	Vdac2	32	105	2
Voltage-dependent anion channel protein 3	Vdac3	31	81	4
MICOS complex subunits				
Mic60/Mitofilin/MICOS complex subunit	Immt	76	438	65
Mic19 MICOS complex subunit	Chchd3	26	31	13
Mic26 MICOS complex subunit	Apoo	23	46	-
Mic13 MICOS complex subunit	Mic13	13	31	-
Mic27 MICOS complex subunit	Apool	29	37	-
Sorting and assembly machinery component 50	Samm50	52	110	9
Cyclophilin D/Peptidyl-prolyl cis-trans isomerase F	Ppif	22	88	9

respiratory chain and collapse of the ATP-generating membrane potential leading to the opening of the mitochondrial permeability transition pore (mPTP) [12]. Opening of the mPTP is a pivotal event also known to be triggered by ROS generation and/or Ca^{2+} overload, which activates cell death by apoptosis [18]. Therefore, we determined the role of MPV17 in regulating the opening of the mPTP after I/R. Remarkably, we found that Mpv17^{mut} cardiac mitochondria did not exhibit any notable differences in ROS production both before and after I/R, compared to WT (**Figure 4A**, **4B**), indicating similar ROS generation between the groups even after I/R insult. Although studies in cells and other organs have noted conflicting ROS fluctuations in MPV17 mutants [4, 5, 32], we did not observe this phenotype in the heart. Furthermore, we found that Mpv17^{mut} and WT mice hearts have similar protein levels of ETC sub-

units, for components encoded by both nuclear and mitochondrial DNA (**Figure 5**). In other organs like the kidneys and brain where mtDNA levels are also not greatly affected by MPV17 mutation, Dalla Rosa et al. [10] observed that ETC subunit content and activity also remained relatively constant. They only observed content changes in the liver, which has significantly depleted mtDNA. We assessed the mitochondrial response to Ca^{2+} overload using mitochondrial calcium retention capacity (CRC), where higher CRC is indicative of healthier mitochondria that are better able to resist calcium-induced mPTP opening. We found that again, normal/non-ischemic Mpv17^{mut} mitochondria have similar CRC to WT mitochondria, but remarkably, this capacity is significantly reduced after I/R in Mpv17^{mut} compared to WT (**Figure 4C**, **4D**). This result suggests that post-ischemia, Mpv17^{mut} mitochondria are more sus-

ceptible to damage caused by Ca^{2+} overload that leads to mPTP opening. Opening of the mPTP in response to I/R promotes cell death *via* the release of cytochrome C and AIF into the cytosol. **Figure 6G** shows an increase in the release of cytochrome C and AIF into the cytosol after I/R compared to sham. This result is consistent with I/R insult promoting mPTP opening in both groups, however, the Mpv17^{mut} released more AIF compared to the WT, suggesting an AIF-reliant pathway being dominant in the mutants. Taken together, our results indicate a mitochondrial damage mechanism in Mpv17^{mut} mice hearts that is more dependent on mitochondrial Ca^{2+} homeostasis than ROS generation, as ROS production between Mpv17^{mut} and WT was similar.

Presently, the molecular structure of the mPTP is still being debated with Cyclophilin D (CypD) being the only known regulator of this large pore whose opening leads to mitochondrial depolarization and cell death [19, 23]. We performed mass spectrometric screen of MPV17 pulldown and revealed hundreds of fragments that were uniquely matched to more than 260 different proteins (Data not shown) including ATP synthase subunits and other inner mitochondrial membrane (IMM) proteins (**Table 2**). From this list, we focused on proteins with the highest abundance: ATP synthase alpha subunit (Atp5a), ATP synthase beta subunit (Atp5b), and GRP75 (mitochondrial Hsp70/mortalin; Hspa9). Additionally, we also identified CypD (Ppif), the known regulator of mPTP opening, as well as Mic60 (Mitofilin, Immt), the main component of the mitochondrial contact site and cristae organizing system (MICOS) that regulates cristae morphology in mammalian mitochondria [28]. To confirm the interaction between MPV17 and these IMM proteins, we conducted reverse co-immunoprecipitation with each protein and affirmed a link between MPV17 and each of these proteins: ATPase, CypD, Mic60 and GRP75 (**Figure 6**, and Mass spectrometry data in **Table 2**). Although debatable, it has been hypothesized that ATP synthase (ATPase, ETC complex V) may be part of the mPTP [33-36]. Our data suggests that there is indeed an interaction between MPV17, ATPase and CypD in the IMM and further supporting this result is the fact that ATPase is a complex of approximately 600 kDa, which matches with the observed unidentified complex like seen by Dallabona et al. [24]. However, our findings do not propose ATPase, nor MPV17, to be components of the mPTP, as this requires further studies. Our data does rather indicate that in cardiac tissue, MPV17 links with ATPase, possibly at the F1 subunit where the α and β subunits reside, along with CypD, and that these interactions are decreased after I/R injury (**Figure 6**). Furthermore, it is known that ATPase dimerization allows for cristae folding in the IMM [37, 38] and that MICOS, and in particular, Mic60, is the main regulator of cristae morphology [28]. We found that MPV17 interacts with ATPase and MICOS subunits, which could explain the destruction of mitochondrial cristae structure after I/R that we observed (**Figure 3**). Supplementing the notion of MPV17 impacting Ca^{2+} homeostasis, we found that MPV17 interacts with the chaperone, glucose-regulated protein 75 (GRP75) (**Table 2**) that mediates endoplasmic reticulum (ER)-mitochondrial interactions [39], especially in preventing cell death during mitochondrial Ca^{2+} overload [40]. GRP75 is also the key link that connects the ER's inositol 1,4,5-triphosphate receptor (IP3R) to the outer mitochondrial membrane's voltage-dependent anion channel 1 (VDAC1) [41], which we also found to interact with MPV17 (**Table 2**). Hence, a limitation of our approach is that it does not resolve how MPV17, an IMM protein, interacts with outer membrane proteins like VDAC, but this could potentially be through multimeric complexes and intermediaries such as GRP75. Our results were obtained using a full-body mutant (not cardiac-specific) with hepatic dysfunction, which might promote cardiomyocyte susceptibility to stress, which is not seen in basal conditions probably due to systemic compensatory mechanisms *in vivo*. It is possible that after I/R, exacerbation of stress abridges this compensatory mechanism leading to the damage we observed.

Conclusion

We report that cardiac MPV17 is a critical interactor with IMM proteins, which are responsible for mitochondrial function, cristae morphology and mPTP opening (**Figure 7**). The reduction or loss of these interactions through MPV17 mutation results in critical failure of mitochondria to regulate Ca^{2+} homeostasis during stresses such as I/R. This leads to increased mitochondrial sensitivity to Ca^{2+} overload that promotes mPTP opening and subsequently causes cardiomyocyte death.
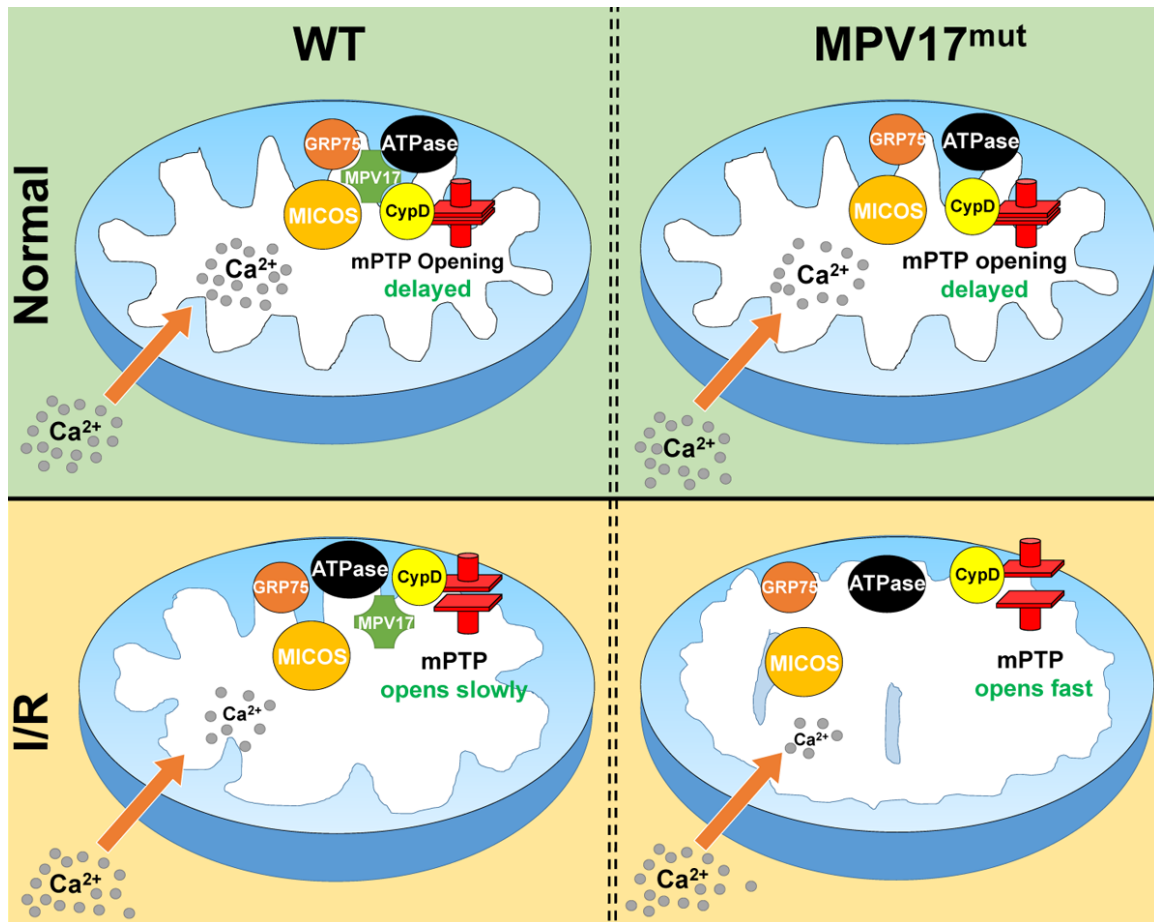
Figure 7. Schematic diagram showing how lack of MPV17 affects mPTP regulation. Lack of functional MPV17 in mutant mice hearts (Mut) results in more mitochondrial damage and increased susceptibility to mitochondrial permeability transition pore (mPTP) opening by calcium overload after I/R. This is because MPV17 is not able to scaffold the mitochondrial proteins: ATP synthase (ATPase), GRP75, cyclophilin D (CypD) and the mitochondrial contact site and cristae organizing system (MICOS).

Disclosure of conflict of interest

None.

Abbreviations

MDS, mitochondrial DNA depletion syndromes; I/R, ischemia/reperfusion; mtDNA, mitochondrial DNA; mPTP, mitochondrial permeability transition pore; CRC, calcium retention capacity; ROS, reactive oxygen species; MICOS, mitochondrial contact site and cristae organizing system; AIF, apoptosis-inducing factor; ROC, rate of oxygen consumption; LDH, lactate dehydrogenase.

Address correspondence to: Dr. Jean C Bopassa, Department of Cellular & Integrative Physiology, School of Medicine, The University of Texas Health at San Antonio, 7703 Floyd Curl Dr. San Antonio, TX 78229, USA. Tel: 210-567-0429; Fax: 210-567-4410; E-mail: bopassa@uthscsa.edu

References

[1]   Weiher H, Noda T, Gray DA, Sharpe AH and Jaenisch R. Transgenic mouse model of kidney

disease: insertional inactivation of ubiquitously expressed gene leads to nephrotic syndrome. Cell 1990; 62: 425-434.

[2] El-Hattab AW, Wang J, Dai H, Almannai M, Staufner C, Alfadhel M, Gambello MJ, Prasun P, Raza S, Lyons HJ, Afqi M, Saleh MAM, Faqeih EA, Alzaidan HI, Alshenqiti A, Flore LA, Hertecant J, Sacharow S, Barbouth DS, Murayama K, Shah AA, Lin HC, Wong LC. MPV17-related mitochondrial DNA maintenance defect: New cases and review of clinical, biochemical, and molecular aspects. Hum Mutat 2018; 39: 461-470.

[3] Shvetsova AN, Mennerich D, Keratar JM, Hiltunen JK and Kietzmann T. Non-electron transfer chain mitochondrial defects differently regulate HIF-1alpha degradation and transcription. Redox Biol 2017; 12: 1052-1061.

[4] Antonenkov VD, Isomursu A, Mennerich D, Vapola MH, Weiher H, Kietzmann T and Hiltunen JK. The human mitochondrial DNA depletion syndrome gene MPV17 encodes a non-selective channel that modulates membrane potential. J Biol Chem 2015; 290: 13840-13861.

[5] Zwacka RM, Reuter A, Pfaff E, Moll J, Gorgas K, Karasawa M and Weiher H. The glomerulosclerosis gene Mpv17 encodes a peroxisomal protein producing reactive oxygen species. EMBO J 1994; 13: 5129-5134.

[6] Qualls C, Kornfeld M, Joste N, Ali AM and Appenzeller O. MPV17-related hepatocerebral mitochondrial DNA depletion syndrome (MPV17-NNH) revisited. eNeurologicalSci 2016; 2: 8-13.

[7] Bitting CP and Hanson JA. Navajo neurohepatopathy: a case report and literature review emphasizing clinicopathologic diagnosis. Acta Gastroenterol Belg 2016; 79: 463-469.

[8] Spinazzola A, Viscomi C, Fernandez-Vizarra E, Carrara F, D'Adamo P, Calvo S, Marsano RM, Donnini C, Weiher H, Strisciuglio P, Parini R, Sarzi E, Chan A, DiMauro S, Rotig A, Gasparini P, Ferrero I, Mootha VK, Tiranti V and Zeviani M. MPV17 encodes an inner mitochondrial membrane protein and is mutated in infantile hepatic mitochondrial DNA depletion. Nat Genet 2006; 38: 570-575.

[9] Viscomi C, Spinazzola A, Maggioni M, Fernandez-Vizarra E, Massa V, Pagano C, Vettor R, Mora M and Zeviani M. Early-onset liver mtDNA depletion and late-onset proteinuric nephropathy in Mpv17 knockout mice. Hum Mol Genet 2009; 18: 12-26.

[10] Dalla Rosa I, Camara Y, Durigon R, Moss CF, Vidoni S, Akman G, Hunt L, Johnson MA, Grocott S, Wang L, Thorburn DR, Hirano M, Poulton J, Taylor RW, Elgar G, Marti R, Voshol P, Holt IJ and Spinazzola A. MPV17 Loss causes deoxynucleotide insufficiency and slow DNA repli-

cation in mitochondria. PLoS Genet 2016; 12: e1005779.

[11] Zhou YQ, Foster FS, Parkes R and Adamson SL. Developmental changes in left and right ventricular diastolic filling patterns in mice. Am J Physiol Heart Circ Physiol 2003; 285: H1563-1575.

[12] Madungwe NB, Zilberstein NF, Feng Y and Bopassa JC. Critical role of mitochondrial ROS is dependent on their site of production on the electron transport chain in ischemic heart. Am J Cardiovasc Dis 2016; 6: 93-108.

[13] Feng Y and Bopassa JC. Oxygen surrounding the heart during ischemic conservation determines the myocardial injury during reperfusion. Am J Cardiovasc Dis 2015; 5: 127-139.

[14] Rahman S, Li J, Bopassa JC, Umar S, Iorga A, Partownavid P and Eghbali M. Phosphorylation of GSK-3beta mediates intralipid-induced cardioprotection against ischemia/reperfusion injury. Anesthesiology 2011; 115: 242-253.

[15] Bopassa JC, Eghbali M, Toro L and Stefani E. A novel estrogen receptor GPER inhibits mitochondria permeability transition pore opening and protects the heart against ischemia-reperfusion injury. Am J Physiol Heart Circ Physiol 2010; 298: H16-23.

[16] Bopassa JC, Ferrera R, Gateau-Roesch O, Couture-Lepetit E and Ovize M. PI 3-kinase regulates the mitochondrial transition pore in controlled reperfusion and postconditioning. Cardiovasc Res 2006; 69: 178-185.

[17] Ferrera R, Bopassa JC, Angoulvant D and Ovize M. Post-conditioning protects from cardioplegia and cold ischemia via inhibition of mitochondrial permeability transition pore. J Heart Lung Transplant 2007; 26: 604-609.

[18] Kabir ME, Singh H, Lu R, Olde B, Leeb-Lundberg LM and Bopassa JC. G protein-coupled estrogen receptor 1 mediates acute estrogen-induced cardioprotection via MEK/ERK/GSK-3beta pathway after ischemia/reperfusion. PLoS One 2015; 10: e0135988.

[19] Feng Y, Madungwe NB, da Cruz Junho CV and Bopassa JC. Activation of G protein-coupled oestrogen receptor 1 at the onset of reperfusion protects the myocardium against ischemia/reperfusion injury by reducing mitochondrial dysfunction and mitophagy. Br J Pharmacol 2017; 174: 4329-4344.

[20] Assaly R, de Tassigny A, Paradis S, Jacquin S, Berdeaux A and Morin D. Oxidative stress, mitochondrial permeability transition pore opening and cell death during hypoxia-reoxygenation in adult cardiomyocytes. Eur J Pharmacol 2012; 675: 6-14.

[21] Das DK, Maulik N, Sato M and Ray PS. Reactive oxygen species function as second mes-

senger during ischemic preconditioning of heart. Mol Cell Biochem 1999; 196: 59-67.

[22] Mishra J, Davani AJ, Natarajan GK, Kwok WM, Stowe DF and Camara AKS. Cyclosporin A increases mitochondrial buffering of calcium: an additional mechanism in delaying mitochondrial permeability transition pore opening. Cells 2019; 8: 1052.

[23] Baines CP, Kaiser RA, Purcell NH, Blair NS, Osinska H, Hambleton MA, Brunskill EW, Sayen MR, Gottlieb RA, Dorn GW, Robbins J and Molkentin JD. Loss of Cyclophilin D reveals a critical role for mitochondrial permeability transition in cell death. Nature 2005; 434: 658-662.

[24] Dallabona C, Marsano RM, Arzuffi P, Ghezzi D, Mancini P, Zeviani M, Ferrero I and Donnini C. Sym1, the yeast ortholog of the MPV17 human disease protein, is a stress-induced bioenergetic and morphogenetic mitochondrial modulator. Hum Mol Genet 2010; 19: 1098-1107.

[25] El-Hattab AW, Suleiman J, Almannai M and Scaglia F. Mitochondrial dynamics: biological roles, molecular machinery, and related diseases. Mol Genet Metab 2018; 125: 315-321.

[26] Puchelle E, Hinnrasky J, Tournier JM and Adnet JJ. Ultrastructural localization of bronchial inhibitor in human airways using protein A-gold technique. Biol Cell 1985; 55: 151-154.

[27] El-Hattab AW and Scaglia F. Mitochondrial cytopathies. Cell Calcium 2016; 60: 199-206.

[28] Feng Y, Madungwe NB and Bopassa JC. Mitochondrial inner membrane protein, Mic60/Mitofilin in mammalian organ protection. J Cell Physiol 2019; 234: 3383-3393.

[29] Lollgen S and Weiher H. The role of the Mpv17 protein mutations of which cause mitochondrial DNA depletion syndrome (MDDS): lessons from homologs in different species. Biol Chem 2015; 396: 13-25.

[30] Madungwe NB, Feng Y, Lie M, Tombo N, Liu L, Kaya F and Bopassa JC. Mitochondrial inner membrane protein (Mitofilin) knockdown induces cell death by apoptosis via an AIF-PARP-dependent mechanism and cell cycle arrest. Am J Physiol Cell Physiol 2018; 315: C28-C43.

[31] Clozel M, Hess P, Fischli W, Loffler BM, Zwacka RM, Reuter A and Weiher H. Age-dependent hypertension in Mpv17-deficient mice, a transgenic model of glomerulosclerosis and inner ear disease. Exp. Gerontol 1999; 34: 1007-1015.

[32] Binder CJ, Weiher H, Exner M and Kerjaschki D. Glomerular overproduction of oxygen radicals in Mpv17 gene-inactivated mice causes podocyte foot process flattening and proteinuria: a model of steroid-resistant nephrosis sensitive to radical scavenger therapy. Am J Pathol 1999; 154: 1067-1075.

[33] Baines CP and Gutierrez-Aguilar M. The still uncertain identity of the channel-forming unit(s) of the mitochondrial permeability transition pore. Cell Calcium 2018; 73: 121-130.

[34] Biasutto L, Azzolini M, Szabo I and Zoratti M. The mitochondrial permeability transition pore in AD 2016: an update. Biochim Biophys Acta 2016; 1863: 2515-2530.

[35] Elustondo PA, Nichols M, Negoda A, Thiruma-ran A, Zakharian E, Robertson GS and Pavlov EV. Mitochondrial permeability transition pore induction is linked to formation of the complex of ATPase C-subunit, polyhydroxybutyrate and inorganic polyphosphate. Cell Death Discov 2016; 2: 16070.

[36] Giorgio V, von Stockum S, Antoniel M, Fabbro A, Fogolari F, Forte M, Glick GD, Petronilli V, Zoratti M, Szabo I, Lippe G and Bernardi P. Dimers of mitochondrial ATP synthase form the permeability transition pore. Proc Natl Acad Sci U S A 2013; 110: 5887-5892.

[37] Hahn A, Parey K, Bublitz M, Mills DJ, Zickermann V, Vonck J, Kuhlbrandt W and Meier T. Structure of a complete ATP synthase dimer reveals the molecular basis of inner mitochondrial membrane morphology. Mol Cell 2016; 63: 445-456.

[38] Daum B, Walter A, Horst A, Osiewacz HD and Kuhlbrandt W. Age-dependent dissociation of ATP synthase dimers and loss of inner-membrane cristae in mitochondria. Proc Natl Acad Sci U S A 2013; 110: 15301-15306.

[39] Phillips MJ and Voeltz GK. Structure and function of ER membrane contact sites with other organelles. Nat Rev Mol Cell Biol 2016; 17: 69-82.

[40] Honrath B, Metz I, Bendridi N, Rieusset J, Culmsee C and Dolga AM. Glucose-regulated protein 75 determines ER-mitochondrial coupling and sensitivity to oxidative stress in neuronal cells. Cell Death Discov 2017; 3: 17076.

[41] Szabadkai G, Bianchi K, Varnai P, De Stefani D, Wieckowski MR, Cavagna D, Nagy AI, Balla T and Rizzuto R. Chaperone-mediated coupling of endoplasmic reticulum and mitochondrial Ca^{2+} channels. J Cell Biol 2006; 175: 901-911.